The specific features of the developing T cell compartment of the neonatal lung are a determinant of respiratory syncytial virus immunopathogenesis

Thomas Démoulins[1,2], Melanie Brügger[1,2,3], Beatrice Zumkehr[1,2], Blandina I. Oliveira Esteves[1,2], Kemal Mehinagic[1,2,3,4], Amal Fahmi[1,2,3], Loïc Borcard[1,2,3], Adriano Taddeo[1,2], Horst Posthaus[4,5], Charaf Benarafa[1,2], Nicolas Ruggli[1,2], and Marco P. Alves[1,2,*]

[1]The Institute of Virology and Immunology, Mittelhäusern and Bern, Switzerland

[2]Department of Infectious Diseases and Pathobiology, Vetsuisse Faculty, University of Bern, Bern, Switzerland

[3]Graduate School for Cellular and Biomedical Sciences, University of Bern, Bern, Switzerland

[4]Institute of Animal Pathology, Department of Infectious Diseases and Pathobiology, Vetsuisse Faculty, University of Bern, Bern, Switzerland

[5]COMPATH, Vetsuisse Faculty & Faculty of Medicine, University of Bern, Bern, Switzerland

[*]Corresponding Author: marco.alves@vetsuisse.unibe.ch

Short Title: Atypical neonatal immune response to RSV infection

Descriptor number: 10.09 Pathogen/Host Cell Interactions

Word count abstract: 204

Manuscript word count: 5671

References: 61

Figures: 6

Supplementary material: 5 figures, 2 tables

ABSTRACT

The human respiratory syncytial virus (RSV) is a major cause of severe lower respiratory tract infections in infants, possibly due to the specific features of the immature neonatal pulmonary immune system. Using the newborn lamb, a classical model of human lung development and a state-of-the-art model of RSV infection, we aimed to explore the role of cell-mediated immunity in RSV disease during early life. Remarkably, in healthy conditions, the developing T cell compartment of the neonatal lung showed major differences to that seen in the mature adult lung. The most striking observation being a high baseline frequency of bronchoalveolar IL-4-producing CD4 and CD8 T cells, which declined progressively over developmental age. RSV infection exacerbated this pro-type 2 environment in the bronchoalveolar space, rather than inducing a type 2 response *per se*. Moreover, regulatory T cell suppressive functions occurred very early to dampen this pro-type 2 environment, rather than shutting them down afterwards, while γδ T cells dropped and failed to produce IL-17. Importantly, RSV disease severity was related to the magnitude of those unconventional bronchoalveolar T cell responses. These findings provide novel insights in the mechanisms of RSV immunopathogenesis in early life, and constitute a major step for the understanding of RSV disease severity.

Keywords: Respiratory syncytial virus; neonatal immunity; bronchiolitis; interstitial pneumonia, immunopathogenesis; Cell-mediated immunity, T cells.

AUTHOR SUMMARY

By using a state-of-the-art translational model with full accessibility to the small airways at defined early life periods, we provide an unpreceded characterization of the developing T cell compartment in the distal lungs of healthy and RSV-infected neonates. This process is highly dynamic and tightly regulated, characterized by colonizing T-cell subsets that synergize towards a narrow pro-tolerogenic immunological window. We believe our work constitutes a solid basis to clarify the age dependency of RSV immunopathogenesis, and should be considered in vaccine design, which remains challenging after five decades of effort.

56 **INTRODUCTION**

57 The human respiratory syncytial virus (RSV) is a seasonal virus, known as the major cause of
58 lower respiratory tract infection during early childhood (1, 2). Worldwide, RSV leads to around
59 160'000 deaths each year (3). Although there are risk factors for RSV severity such as
60 prematurity and congenital heart disease, the majority of hospitalized infants are previously
61 healthy (4-7), suggesting that the disease is partially linked to inherent properties of early life
62 immunity. The precise understanding of the immune-driven susceptibility of neonates is
63 essential, considering there is no licensed vaccine and available prophylactic treatments are
64 mostly based on palivizumab, a neutralizing antibody used in high-risk group infants (8).

65 The first exposure to pathogens occurs during the early postnatal period and is critical for lung
66 colonization by immune cells. There is increasing evidence that the overall neonatal T-cell
67 compartment is distinctive during this temporal window (9). Upon stimulation neonatal T-cells
68 tend to differentiate into regulatory T-cells (Tregs), to facilitate self-tolerance to developing
69 organs (10). Also, the developing lung is characterized by a type 2 immune phenotype, and
70 the pulmonary T-cell responses present a T helper type 2 (Th2) bias (11, 12). Remarkably,
71 neonatal $\gamma\delta$ T-cells, a T-cell subset enriched at mucosal barrier sites, have an impaired
72 capacity to respond to stimulation (13-16).

73 Due to the aforementioned reasons, young infants do not mount a classical pulmonary
74 immune response to pathogens such as RSV, which may contribute to high morbidity and
75 mortality (17, 18). A likely explanation could be a combined contribution of viral load (19) and
76 an inappropriate and/or dysfunctional immune response, through an over-exuberant
77 inflammatory response or a biased T-cell response (9, 20, 21). Neonatal T-cells may have
78 both protective and harmful effects in responses to RSV infection. While children with T-cell
79 deficiencies cannot efficiently clear the virus (22, 23), it remains controversial whether the
80 severity of RSV disease is associated with a bias towards type 2 cytokines such as IL-4 (24-
81 26).

82 Knowledge of the course of RSV disease is still limited due to ethical and technical difficulties
83 associated with the investigation of the immune response in human neonates. The neonatal
84 lamb model of human RSV infection recapitulates most of the features of the paediatric
85 disease. Furthermore, due to similarities in development and pulmonary immune system, the
86 ovine lung is a classical model of the human respiratory tract (27). Human RSV-infected
87 animals clinically present rhinitis, coughing and respiratory distress. Typical pulmonary lesions
88 are bronchiolitis and interstitial pneumonia associated with inflammatory infiltrates (28-30).
89 Herein, this model, immunologically related to human, was exploited to have full access to the
90 small airways and follow the development of the pulmonary immune cell features in early life.
91 Moreover, by peribronchial lymph nodes (LNs), lung, and bronchoalveolar space sampling
92 following RSV infection, we provided an unprecedented delineation of the contributors of the
93 host neonatal T cell compartment over the course of RSV disease.
94

95 **RESULTS**

96 **RSV infection is causing lower respiratory tract disease and leading to a potentially**
97 **protective humoral response**

98 To evaluate the immune responses during the acute, recovery and convalescence phases of
99 RSV disease, time-points were Selected as follow: 3 and 6 days post-infection (p.i.), to
100 evaluate the innate and early adaptive responses; 14 days p.i. to assess the adaptive
101 mechanisms and virus clearance; 42 days p.i. to investigate the impact of RSV infection on
102 the immune cell colonization of the developing lung. As controls, non-infected newborns and
103 adults were used (Figure 1A). We quantified RSV in BALs (cellular and fluid fractions) and in
104 the lung tissue. Although RSV clearance was slower in the cellular fraction of BALs, it became
105 undetectable in any sample at day 42 p.i., demonstrating an efficient clearance (Figure 1B).
106 Immunohistochemistry of lung tissue sections revealed the presence of RSV-antigens in type
107 I pneumocytes and macrophages (Figure 1C). Clinically, RSV infected neonates showed signs
108 of rhinitis with clear nasal discharge, occasional coughing and wheezing. Macroscopical

109 lesions were visible at days 3-6 p.i, including failure of pulmonary collapse and focal, dark-red
110 areas of subpleural pulmonary consolidation and atelectasis. Histological lesions, present at
111 days 3-6 p.i consisted of multifocal-coalescing areas of lymphocytic and histiocytic infiltrates
112 within interalveolar septae (interstitial pneumonia) and accumulation of inflammatory cells
113 within alveolar spaces and bronchioles (bronchiolitis) (Figure 1D). Longitudinal measurements
114 of white blood counts and neutrophil counts in the circulation showed no difference between
115 mock and infected neonates (Figure S1). Next, we monitored the presence of RSV neutralizing
116 antibodies (NAbs) (Figures 1E, S2). In the serum of healthy adults and mock neonates, no
117 RSV NAbs were detected. In contrast, RSV-infected neonates have naturally acquired NAbs
118 at day 13-14 p.i., except one animal. Notably, two siblings had RSV NAbs preceding infection;
119 this was passively transmitted by their mother whose serum also had a strong RSV-
120 neutralization (Figure S3). We extended the assay to later time points to test the persistence
121 of RSV neutralization. No loss of humoral memory was measured up to 42 days p.i (Figure
122 1F). Altogether, these results indicate that neonates can mount an efficient humoral response
123 suggesting potential protection for a subsequent RSV infection. When quantifying the cytokine
124 profiles in BALs from mock control and RSV-infected animals, the most noticeable induction
125 upon infection were IL-10 (day 6 p.i.), IL-8 and CXCL10/IP-10 (days 3 and 6 p.i.). The latter
126 being a potent lymphocyte chemoattractant (Figure 1G).
127

128 **Neonatal RSV infection leads to a transient depletion of γδ T cells and a deficiency of**
129 **IL-17-mediated immunity**

130 We first assessed central components of the pulmonary immune responses bridging innate
131 and adaptive responses, namely plasmacytoid DCs (pDCs) and γδ T cells. In RSV disease,
132 pDCs are known to be involved during the early stages of the pulmonary immune response
133 and have a protective function by modulating the local immune microenvironment (31). When
134 quantified in the BALs, pDC numbers of mock neonates were similar to those of healthy adults.
135 Upon RSV infection, we observed a trend to pDC recruitment as early as 3 days p.i., and this

136 was enhanced at day 6 p.i. ($p<0.05$). This recruitment was specific of bronchoalveolar space,
137 since we failed to detect any increase in peribronchial LN and lung tissue. However, the pDC
138 recruitment in the bronchoalveolar space was transitional and tightly regulated, since day 14
139 p.i corresponded to a return to steady-state levels (Figure S4A, S5A). To verify whether the
140 extent of pDC recruitment was linked to the magnitude of RSV shedding, pDC counts were
141 plotted as a function of RSV copies in the fluid fraction of BALs. A significant association was
142 found (Figure S5B). We next evaluated the maturation and activation phenotype of recruited
143 pDCs. A significant CD86 upregulation was found at days 3-6 p.i. (Figure S5C, D). This
144 upregulation was transitional and back to steady-state levels at day 14 p.i. In line with the early
145 pDC recruitment and activation, we observed a significant upregulation of IFN-β during the
146 acute phase of neonatal RSV infection, suggesting the induction of an antiviral state in the
147 respiratory tract (Figure S5E).
148 Similar to pDCs, γδ T cells link the innate and adaptive arms of the immune system, particularly
149 at mucosal sites including the respiratory tract. Thus, we wondered whether they were
150 involved in the early immune response to RSV infection (32). γδ T cell numbers in the
151 peribronchial LNs, lung tissue and BALs of mock neonates were comparable to those
152 calculated in healthy adults. However, neonatal RSV infection led to a noticeable decrease in
153 γδ T cell frequency in the BALs at day 14 p.i., whereas this remained stable in other lung
154 compartments. Nevertheless, this γδ T cell depletion was entirely reversed at day 42 p.i.
155 (Figure 2A, S4A). To exclude the possibility that the γδ T cell reduction could be due to
156 migration or relocation, we calculated their counts as a function of the percentage of
157 Live/Dead-positive cells. A negative association was found, suggesting that neonatal γδ T cells
158 death is linked to the presence of RSV in the bronchoalveolar space (Figure 2B). We next
159 ascertained whether neonatal γδ T cells in BALs remained immature during the recovery
160 phase. Remarkably, in healthy adults, half of the γδ T cell pool was composed of mature $CD25^+$
161 cells, whereas the latter were absent in mock neonates at day 3. The proportion of mature γδ
162 T cells progressively strengthened over time, without reaching the level detected in healthy

163 adults. RSV infection exerts an effect on this maturation of neonatal γδ T cells. Not only the
164 observed depletion was rapidly followed by a complete replenishment at day 42 p.i., but also
165 the restoration was accompanied by a marked increase in the percentage of CD25-positive
166 cells, compared to mock neonates (Figure 2C, D). Finally, we demonstrated the inability of
167 neonatal γδ T cells to produce detectable levels of IL-17 (Figure 2E).
168
169 **Neonatal RSV infection induces a fast and massive Tc2 influx in the bronchoalveolar**
170 **space**
171 Assessment moved on to adaptive immune response, and more particularly to IL-4 *versus*
172 IFN-γ production by $CD4^+$ or $CD8^+$ T cells, a determining factor in the outcome of protective
173 *versus* harmful immune response to RSV infection (25, 33) (Figure 3A, S4C). In BALs, mock
174 neonates had a very low number of $CD4^+$ and $CD8^+$ T-cells compared to healthy adults,
175 whereas numbers were comparable in draining LNs. RSV infection led to their strong
176 recruitment in the bronchoalveolar space, albeit with distinct kinetics. An unexpected reduction
177 of $CD4^+$ T-cell recruitment was seen as soon as 14 days p.i. This contradicted the values
178 obtained for $CD8^+$ T-cells, where the significant enhancement following RSV infection was
179 maintained. Interestingly, this influx of $CD8^+$ T cells was preceded by their significant increase
180 in the lung, indicating that they transit through this compartment. When we considered both
181 $CD4^+$ and $CD8^+$ fractions at a later time-point, the numbers were comparable to those of mock
182 neonates (Figure 3B). Surprisingly, mock neonates had high baseline frequencies of Th2 cells
183 in BALs, which declined progressively over time. Elevated amounts of spontaneous produced
184 IL-4 were a signature of the developing $CD4^+$ fraction, since it was no longer detectable at day
185 42, or in healthy adults. Upon infection, this analysis revealed a trend towards an increase in
186 the frequency of those Th2 cells, whereas there was no consistent influence on IFN-γ induction
187 (Figures 3C, D). Consequently, RSV infection in early life exacerbates the overall lung pro-
188 Th2 cytokine environment, rather than inducing a Th2 immune response *per se*.

189 High baseline frequencies of IL-4-expressing $CD8^+$ T-cells (Tc2) were also found in BALs of
190 in mock neonates. Again, a progressive decline of Tc2 cells occurred up to day 42 p.i.,
191 comparable to negligible levels measured in healthy adults. RSV disease induced a greater
192 overall Tc2-derived cytokine environment in BALs. This exacerbation was tightly regulated,
193 reduced to a level similar to healthy adults at day 14 p.i. Again, no consistent influence of RSV
194 infection was seen on IFN-γ induction (Figure 3E, F). Altogether, these results highlight the
195 role of Tc2 cells as an important source of IL-4 production during neonatal RSV infection.
196 Finally, we then tested the activation and differentiation of naïve T lymphocytes into memory
197 subsets. The most striking observation was achieved at day 42 p.i.; the percent contributions
198 of different subsets seen in RSV-infected neonates was highly superimposable to that found
199 in healthy adults. This was not the case for mock neonates who had lower frequencies of
200 activated memory T-cells, particularly for the $CD8^+$ fraction (Figure 3G). Consequently, RSV
201 infection in early life modulates the activation and the maturation of the T-cell pool.
202 Nonetheless, it is unknown whether this precipitated activation/maturation is RSV epitope-
203 specific and a predictive factor for severe outcomes in the context of a secondary RSV
204 infection (34).
205
206 **Neonatal RSV infection rapidly induces Treg suppressive functions to dampen the Th2**
207 **and Tc2 responses**
208 The neonatal immune system is tolerogenic, a mechanism that promotes self-tolerance to
209 developing organs; fetal $CD4^+$ T cells are more likely to differentiate into Tregs after stimulation
210 (10). The shortened kinetics observed for $CD4^+$ T-cells was elaborated by determining whether
211 this was due to an early Treg rather than a classical $CD4^+$ T-cell response (Figure 4A, S4D).
212 RSV infection elicited a rapid Treg recruitment in BALs that mirrored the one previously
213 observed for $CD4^+$ T-cells. This Treg dynamic is specific for the respiratory mucosa, since
214 Treg frequencies remained unchanged in the lung tissue (Figure 4A). We then noticed a trend
215 for Treg subset overrepresentation following RSV infection (Figure 4B). The proportion of
216 Tregs declined progressively over time, tending towards similar levels to those detected in

217 healthy adults. RSV infection promoted enhancement of TGF-β production by Tregs, however
218 not significant (Figure 4C). When Treg counts were calculated as a function of non-Treg $CD4^+$
219 counts, an association was found, suggesting that $CD4^+$ T-cell pool tends to differentiate into
220 Tregs. When Treg counts were calculated as a function of $CD8^+$ counts, an association was
221 still found, confirming that $CD8^+$ T-cells and Tregs colonized the alveolar space in a
222 coordinated manner. By plotting $CD8^+$ count as a function of non-Tregs $CD4^+$ counts, it
223 appeared that T-cell response was mainly driven by the $CD8^+$ fraction (high numbers at days
224 6 and 14 p.i.) (Figure 4D).
225
226 **Neonates and adults are mounting a distinct pulmonary T cell response following RSV**
227 **infection**
228 We followed the same approach to dissect the cellular immune response in RSV-infected
229 adults. While the viral loads and virus clearance was comparable between adults and
230 neonates (Figure 5A), respiratory lesions were absent in adults (Figure 5B); this suggests that
231 the increased rate of severe disease reported in infants is not due to a failure to control the
232 virus, reinforcing the hypothesis for immune-mediated RSV pathogenesis.
233 The rapid and robust pDC recruitment observed in infected neonates did not occur in infected
234 adults. However, lung-resident pDCs of the latter were prompt to react, displaying an even
235 more mature and activated phenotype Importantly, this mature pDC response was also tightly
236 regulated (Figure 5C, D). The strong decrease in γδ T-cell counts observed in infected
237 neonates was absent in adults. Moreover, adult γδ T-cells produced high amounts of IL-17,
238 suggesting that IL-17-mediated immunity is deficient in early life (Figure 5E, F) (15). This IL-
239 17 response was accompanied by an activated phenotype, as indicated by the enhanced
240 proportion of $CD25^+$ cells (Figure 5G). From these results, we could ascertain that neonates
241 lack a mature and functional γδ T-cell pool in the lower airways. For the $CD4^+$ subset, no
242 significant recruitment was found (Figure 5H). The percentage of IL-4-producing cells was
243 very low, and RSV infection had no consistent influence on IFN-γ induction (Figure 5I). Another

244 clear difference was the contraction of effector memory pool ($CD25^+CD45RO^+$) at day 14 p.i.,
245 indicative of a specific immune response (Figure 5J). The recruitment of $CD8^+$ T-cells was
246 delayed compared to neonates, only detectable at day 14 p.i. (Figure 5K). Again, the
247 percentage of IL-4-producing cells was low (Figure 5L), whereas the precipitous contraction
248 of effector memory pool at day 14 p.i. suggested a RSV-specific $CD8^+$ T-cell response (Figure
249 5M). From these results, it became clear that the inaptitude of neonates to mount an effector
250 T-cell response is tentatively substituted by a fast and massive Th2/Tc2 cell recruitment.
251 Finally, we failed to detect any Treg recruitment. However, the rare tissue-resident Tregs were
252 able to produce TGF-β, suggesting that an immune regulation happened (Figure 5N, O).
253
254 **The severity of RSV disease relates to the magnitude of the bronchoalveolar T cell**
255 **responses**
256 The pulmonary T-cell response was evaluated in neonates infected with RSV-ON1-H1 strain,
257 which induced a milder disease (Figure 6A). Interestingly, the viral loads and virus clearance
258 was comparable between both strains, again reinforcing the hypothesis for immune-mediated
259 RSV pathogenesis (Figure 6B). Effectively, all T cell-related responses were attenuated. We
260 did not observe a γδ T-cell depletion, and the $CD8^+$ T-cell recruitment was delayed.
261 Furthermore, the Treg recruitment was lower compared to RSV A2 infection (Figure 6C). By
262 combining results obtained with both strains, we found a significant association between Treg
263 and pDC counts in BALs (Figure 6D). This indicates that, despite their skew, all distinct
264 subsets of neonatal T-cells cooperate tightly with the magnitude of the cellular immune
265 response against RSV infection. Altogether, our data clarified how neonates elicit an over-
266 exuberant pulmonary T cell response characterized by a bronchoalveolar influx of Treg, Th2,
267 and Tc2 cells, contrasting to a classical T cell response.
268
269 **DISCUSSION**

270 To properly assess the immunopathogenesis of RSV, it is essential to select a model that
271 recapitulates the features of human disease. We selected the neonatal lamb, as RSV is a
272 natural pathogen for this species, lung development is similar, and the key features mimic
273 human RSV infection in infants (28, 29). One strength of our experimental approach was the
274 ease sampling and the full accessibility to the lower airways throughout the disease when
275 sampling in infants is mainly restricted to the upper airways, the latter representing only an
276 approximate surrogate of the distal lung where RSV disease occurs. Moreover, we offer an
277 unprecedented view of the development of pulmonary neonatal immunity in healthy
278 conditions. This process is highly dynamic and tightly regulated, with a short and early stage
279 where colonizing T-cell subsets synergize towards a narrow pro-tolerogenic window, namely
280 a "Treg/Th2/Tc2" environment. This certainly contributes to the maturation of the immune
281 system and may constitute an unsuitable state to resolve RSV infection.
282 The mechanisms underlying the severity of disease are still unclear, although RSV itself was
283 shown to induce distal lung obstruction by shedding of necrotic airway epithelial cells (35).
284 Also, it is unclear yet if RSV disease severity is associated with viral loads (36, 37). Here we
285 demonstrate that while RSV disease was more severe in neonates compare to adult animals,
286 RSV loads and virus clearance was comparable for both age groups. In line with this, RSV
287 loads and virus clearance were similar for neonates infected with RSV strains inducing an
288 RSV disease with distinct severity. Clearly, our data strongly reinforce the hypothesis of an
289 inappropriate neonatal immune response as a determinant of RSV disease severity. We
290 observed a rapid and robust recruitment of neonatal pDCs, whose extent correlated with the
291 viral loads of infected neonates. Infected adults did not require this recruitment, since their
292 lung-resident pDCs reacted promptly by maturing to a higher level than that measured in
293 neonates. This partially corroborates recent studies reporting low counts and maturation levels
294 of pDCs in mice and infants (38, 39). This reduced capacity to respond against RSV might be
295 due to a direct disturbance of signaling by RSV itself (40), or an intrinsic deficiency of neonatal
296 pDCs to produce elevated amounts of cytokines (41-43). This neonatal defect would prevent

297 conventional DCs from adequate presentation of viral antigens, contributing to poor specific T
298 cell responses (44).
299 Controversial is whether γδ T-cells participate in viral clearance or immunopathology. Herein,
300 the γδ T-cell depletion conflicted with a previous report. Indeed, children with severe RSV
301 bronchiolitis had reduced frequencies of γδ T-cells in peripheral blood, which was explained
302 by the authors as a likely redistribution towards the lungs; unfortunately, they could not
303 evaluate their hypothesis (45). In line with our findings, mice depleted of γδ T-cells before RSV
304 infection display increased viral titers (13). An alternative hypothesis that would reconcile our
305 study with others, is that γδ T-cell tissue redistribution plays less of a role than its immature
306 state in early life. Peripheral blood γδ T-cells of infants with severe disease failed to produce
307 IFN-γ when restimulated (14), whereas γδ T-cells from neonatal mice had an impaired ability
308 to produce IL-17 (15). Finally, Tc17 and Th17 cells were recently associated with shorter
309 hospital stays and proposed to play a protective role (26). Altogether, our data demonstrate
310 that the protective role of γδ T-cells in RSV infection is largely inefficient in early life.
311 The BALs of healthy neonates displayed a high proportion of Tregs that declined rapidly to
312 levels comparable to healthy adults. As fetal $CD4^+$ T-cells tend to differentiate preferentially
313 into Tregs after stimulation (10), this tolerogenic mechanism is likely to promote self-tolerance
314 to the developing lung. We found that Treg response to RSV infection happened very early in
315 neonates, accompanying $CD4^+$ and $CD8^+$ T-cell expansion rather than shutting them down
316 afterwards. This strong Treg recruitment was absent in adults. We speculate that the neonate
317 immune system faces a dilemma between avoiding potential autoimmune disorders and failing
318 to mount a specific T-cell response to harmful pathogens. Studies conducted in young infants
319 with RSV disease support this statement. A selective depletion of peripheral Tregs was shown,
320 probably due to massive recruitment to the lungs (46). A higher level of TGF-β transcript was
321 measured in neonatal DCs compared to adults (47). In contrast, some reports emphasized
322 the protective role of Tregs, since Treg-depleted young mice had an enhanced RSV disease,
323 with abundant T-cells exhibiting an activated phenotype (48). Another remarkable observation

324 was the strong correlation between pDC and Treg counts. Despite the need for further
325 investigations, it is worth noting that pDC to Treg ratio was linked to the clearance *versus*
326 persistence of human papillomavirus (49).
327 Whether the cellular arm of the adaptive pulmonary response is detrimental or beneficial in
328 RSV disease is still debated. Particularly, the contribution of IL-4 to viral clearance versus
329 immunopathogenesis remains controversial (25, 50-52). Recently, a study performed in
330 hospitalized infants showed a possible involvement of Tc2 cells in disease severity. Although
331 convincing, this study was for obvious ethical reasons restricted to nasal aspirates (26).
332 Interestingly, Tc2 cells are increasingly proposed to play an important role in the etiology of
333 asthma (53). Herein, we provide a significant advancement in understanding this yet unclear
334 IL-4 contribution, by showing that type 2 cytokine environment in the lung is a footprint of early
335 life that decreases rapidly with time in healthy conditions. RSV infection circumvents this
336 decline by mediating the massive recruitment of $CD4^+$ and $CD8^+$ T-cells, exacerbating the
337 overall type 2 cytokine environment. We think that the link between IL-4 and RSV disease is
338 the direct consequence of a strong trafficking of endogenous Th2 and Tc2 lymphocytes
339 towards infected pulmonary tissues, rather than an RSV-specific type 2 immune response *per*
340 *se*.
341 The high proportion of pulmonary T-cells producing spontaneously IL-4 was undetectable in
342 the healthy adults. Neither was the RSV-specific immune response of adults oriented towards
343 a Th2 or Tc2 profile. This corroborates a previous report mentioning an endogenously poised
344 cytokine profile toward IL-4 in $CD4^+$ T-cells in cord blood of neonates and infants, establishing
345 a link between IL-4 and development (54). However, we provide new insights by
346 demonstrating that i) $CD8^+$ Tc2 cells are an equal and possibly superior source of IL-4 than
347 $CD4^+$ Th2 cells; ii) this immunological state occurs during a short period *in vivo*, raising the
348 likelihood that numerous animal trials failed to detect it due to the study design. Remarkably,
349 this transient type 2 cytokine environment was exacerbated upon RSV infection. So far, similar
350 observations were only made at the systemic level or in nasal aspirates, and authors could
351 only speculate on the relocation to the lower respiratory tract (26, 55). Herein, not only we

352 show that this happens, but we also unify the link between IL-4 and RSV disease and
353 endogenous IL-4 program in neonates. This finding constitutes an important step towards
354 deciphering why neonates and young infants are particularly at risk.
355 Conclusively, we provid novel insights into the identification of the host's contributing factors
356 to RSV immunopathology, strengthening the hypothesis of an inappropriate immune response
357 in the narrow temporal window of early life. This can now be characterized as a combined
358 bronchoalveolar influx of Treg, Th2 and Tc2 cells, associated with a strong depletion of γδ T
359 cells and IL-17 deficiency. These findings constitute a novel basis for further exploration of
360 RSV immunopathogenesis in infants and should be considered in RSV vaccine design, which
361 remains challenging after five decades of effort.

362

363 **MATERIAL AND METHODS**

364 **Virus**

365 Human RSV-A2 strain was obtained from the American Type Culture Collection (ATCC, VR-
366 1540, GenBank accession number KT992094.1). The strain RSV-ON1-H1 was isolated from
367 nasopharyngeal aspirates of a child below the age of five years with confirmed RSV infection,
368 hospitalized at Hannover Medical School, Germany. The caregivers gave informed consent
369 for the donation of nasopharyngeal aspirates, and all steps were conducted in compliance with
370 good clinical and ethical practice and approved by the local ethical committee at Hannover
371 Medical School (permission number 63090/2012) (56). Both RSV strains were propagated on
372 HEp-2 cells (ATCC, CCL-23) cultured in DMEM (Gibco) supplemented with 5% FBS (Gibco),
373 at 37 °C in 5% CO2 atmosphere. Briefly, viruses were incubated for 36-44 h in tissue culture
374 flasks at a multiplicity of infection (MOI) of 0.02 plaque-forming unit (PFU) per cell. When the
375 cytopathogenic effect (CPE) reached approximately 60%, the cultures were frozen overnight
376 at −70 °C, to disrupt the Hep-2 cells and release the virus. Then, the T-175 cm2 flasks were
377 thawed, HEp-2 cells were scraped and the complete contents of the flask were spun down at
378 1000 g, 10 min, 4 °C to collect cell debris. The clarified supernatants were layered over 20%

379 sucrose (w/v) solution prepared in sterile PBS and ultra-centrifuged for 3 h 30 min at 71'000 g
380 at 4 °C. The resultant RSV stocks were aliquoted and stored at −150 °C until further use.
381 Virus titers were determined on HEp-2 cells, using biotinylated anti-RSV antibody (goat
382 polyclonal IgG, Bio-Rad) for 1 h at RT. The plaques were visualized using ExtrAvidin®-
383 Peroxidase (Sigma), 30 min at RT, and revealed by DAB substrate (Sigma), left for up to 30
384 min at RT. When the plaques appeared with the desired coloration, the reaction was stopped
385 with PBS. RSV titers were expressed as PFU per ml.
386
387 **Animals**
388 The experiments in lambs were performed in compliance with the Swiss animal protection law
389 (TSchG SR 455; TSchV SR 455.1; TVV SR 455.163) under the authorization BE125/17. The
390 experiments were reviewed by the cantonal committee on animal experiments of the canton
391 of Bern, Switzerland, and approved by the cantonal veterinary authority (Amt für
392 Landwirtschaft und Natur LANAT, Veterinärdienst VeD, Bern, Switzerland). For the duration
393 of the experiment, the animals were housed in the high containment animal facility.
394 *Postpartum*, the acclimatization lasted 3 to 6 days before RSV infection. In accordance with
395 the principles of the 3Rs, suckling lambs were held together with their adult mothers and fed
396 *ad libitum*. The animals were kept on straw with a local ambient temperature of 20-22 °C. In
397 order to prevent secondary bacterial infection, all the animals received a prophylactic long-
398 acting oxytetracycline treatment starting at 18 to 24 h before RSV infection by intramuscular
399 injection of Cyclosol LA, 20 mg/kg (Dr. E. Graeub AG), repeated after 4 days. The
400 developmental age of sheep does not follow a linear curve compared to humans but in terms
401 of lung development, animals euthanized at day 3, 6, and 14 post-infection (p.i.) can be
402 considered as infants and at day 42 as adolescents (57). The transtracheal RSV inoculation
403 was performed under sedation and analgesia by intramuscular injection of a mixture of
404 midazolam (Dormicum®, Roche) 0.2 mg/kg and butorphanol (Morphasol®, Dr. E. Graeub AG)
405 0.2 mg/kg. The injection site was shaved and disinfected with 70% ethanol. The trachea was
406 punctured between the proximal tracheal rings with a 0.9 x 40 mm needle (20G, BD) and a

407 volume of 2 ml of virus (RSV-infected animals: 10^8 PFU for RSV-A2; 10^7 PFU for RSV-ON1-
408 H1) or PBS (mock-treated controls) were injected slowly. Before and after infection, we
409 monitored body temperature, and clinical status daily. The clinical status of the lambs was
410 assessed by a veterinarian, whenever possible always the same person to ensure unbiased
411 clinical assessment. The rectal body temperature was measured with a digital thermometer,
412 respiratory and heart rates with a stethoscope.
413
414 **Histopathology and Immunohistochemistry**
415 Samples of each lung lobe were fixed in 10% buffered formalin for 48 h, embedded in paraffin
416 and routinely processed for histology. Three µm Histological sections were stained with
417 hematoxylin and eosin. For Immunohistochemistry, unstained 3 µm sections were
418 deparaffinized with xylol for 5 minutes followed by rehydration in descending concentrations
419 of ethanol (100, 95, 80, and 75%). Endogenous peroxidase activity was inhibited by H_2O_2
420 (3.25% in methanol, 10 min at RT). Then, heat-induced antigen retrieval was carried out by
421 incubating the slides in boiling citrate buffer (pH 6.0) for 10 min. Nonspecific binding of
422 antibody was blocked with 1% BSA for 10 min. Slides were incubated overnight at 4° with
423 primary antibodies diluted 1:200 in PBS (clone 302, ThermoFisher). LSAB and AEC Kits
424 (DakoCytomation) were used as indicated by the manufacturer for secondary antibody
425 incubation and signal detection. Slides were counterstained with Ehrlich hematoxylin and
426 cover slips were mounted using Aquatex (Merck) (58).
427
428 **Cell suspension preparation**
429 The isolation of cells from peribronchial lymph nodes was done using a Collagenase D (Sigma)
430 and DNAse I (BioConcept) enzyme mix and the gentleMACS Octo Dissociator (Miltenyi
431 Biotec). For the isolation of immune cells from the lung tissue, we used a Collagenase I
432 (BioConcept), Collagenase II (BioConcept) and DNase I (BioConcept) enzyme mix. The
433 dissociated tissues were passed through a 100 µm cell strainer (Falcon) and centrifuged at
434 250 g for 10 min, 4 °C. Next, the cell pellets were resuspended, passed through a 70 µm cell

435 strainer (Falcon) to ensure the removal of clumps, and centrifuged 250 g for 10 min, 4 °C. For
436 the lung suspensions, the cells were further purified using the Ficoll-Paque approach (Sigma).
437 For the isolation of cells from bronchoalveolar lavages (BALs), the lungs were taken out with
438 the trachea, which was clamped before cutting, to prevent blood from entering the lungs. Then,
439 PBS was poured through the trachea using a sterile funnel. The single-cell suspensions were
440 applied to a sieve to remove any remaining larger particles. Depending on the BAL volume,
441 single-cell suspensions were distributed in the appropriate number of 50 ml Falcon tubes for
442 centrifugation at 350 g for 10min, 4°C. Then, the pellets were resuspended, passed through a
443 100 µm cell strainer (Falcon) and centrifuged at 350 g for 10 min, 4 °C. Next, the pellets were
444 resuspended, passed through a 70 µm cell strainer (Falcon) to ensure the removal of clumps,
445 and centrifuged at 350 g for 10 min, 4 °C. If needed, red blood cells were lysed by
446 resuspending the pellet with 2 ml of H_2O and washed immediately in cold PBS/EDTA, before
447 centrifugation at 350 g for 10 min, at 4 °C.
448
449 **Human RSV neutralization assay**
450 Serial 2-fold dilutions of heat-inactivated sera (30min, 56°C) were prepared in serum-free
451 DMEM medium, with a starting dilution of 1:4. Serial serum dilutions were incubated at 37 °C
452 for 60 min with an equal volume of RSV to provide 100 PFU per 100 µl. The serum-virus
453 mixtures were added in duplicate to monolayers of HEp-2 cells in 96-well flat-bottom tissue
454 culture-treated microtiter plates and incubated at 37 °C with 5% CO_2 in DMEM 5% FBS. After
455 48 h, cells were washed with 100 µl PBS per well and fixed for 20 min at RT with methanol
456 containing 2% H_2O_2. Cells were washed twice with 100 µl PBS per well, and biotinylated anti-
457 RSV antibody (goat polyclonal IgG, Bio-Rad) was added for 1 h at RT. Cells were washed
458 twice with 100 µl PBS 1% BSA per well and ExtrAvidin®-Peroxidase (Sigma) was added for
459 30 min at RT. Cells were washed twice with 100 µl PBS 1% BSA per well and DAB substrate
460 (Sigma) was added and left up to 30 min at RT. When the plaques appeared with the desired
461 coloration, the reaction was stopped with PBS. Serial two-fold dilutions of Palivizumab®

462 (Synagis), beginning at 100 µg/ml, and virus-free DMEM were used as controls. The plates
463 were scanned with an ImmunoSpot® analyzer (Cellular Technology Limited (CTL)).
464
465 **RNA isolation and quantitative PCR**
466 Total RNA was extracted from BAL fluids using the QiAamp® Viral RNA Mini Kit (QIAgen) and
467 Nucleospin® RNA Plus Kit (Macherey Nagel) for lung tissues and the BAL cellular fraction
468 according to the manufacturer's protocol. For quantitation of RNA expression levels,
469 quantitative PCR (qPCR) was performed using AgPath-ID™ One-Step RT-PCR Reagents
470 (ThermoFisher), according to the manufacturer's instructions. The primer and probe
471 sequences used to detect RSV-A2 and the housekeeping control 18S RNAs have been
472 previously described: RSV-A2 (FW: 5′-GAACTCAGTGTAGGTAGAATGTTTGCA-3′, RV: 5′-
473 TTCAGCTATCATTTTCTCTGCCAAT-3′, Probe: 5′-FAM-
474 TTTGAACCTGTCTGAACATTCCCGGTT-TAMRA-3′) (59); 18S (FW: 5′-
475 CGCCGCTAGAGGTGAAATTCT-3′, RV: 5′-CATTCTTGGCAAATGCTTTCG-3′, Probe: 5′-
476 FAM-ACCGGCGCAAGACGGACCAGA-TAMRA-3′) (60). RNA expression levels of RSV and
477 18S were determined by absolute quantification by the serial dilution of plasmids containing
478 the sequence of interest. For the quantification of interferon-β (IFN-β), primers were designed
479 as follow: FW: 5′-TGGTTCTCCTGCTGTGTTTCTC-3′; RV: 5′-
480 CGTTGTTGGAATCGAAGCAA-3′; Probe: 5′-FAM-ACCACAGCTCTTTCCAGGAGCTACA-
481 BHQ1-3′ (61). For the amplification on ABI Fast 7500 Sequence Detection System (Applied
482 Biosystems), the following conditions were used: 95°C 20 sec, 40-45 cycles of the following:
483 95 °C 3 sec, 60 °C 30 sec, real-time data were analyzed using the SDS software (Applied
484 Biosystems).
485
486 **Flow cytometry**
487 The different ovine immune cell subtypes were identified by flow cytometry (FCM) using an
488 eight-step, seven-color staining protocols. All antibodies used for the procedure, as well as
489 their clones, host, working dilution, and references, are listed in Table E1. Combination

490 stainings analyzed plasmacytoid dendritic cell (pDC), γδ T cells, Tregs, CD4 and CD8 T cell
491 subsets. For the acquisitions, 10^6 events were accumulated for each sample. The
492 experimental schedule is summarized in Table E2. For the counts of cell subtypes, we
493 calculated the percentage of total events: ratio (number of events in the gated cell subtype) to
494 (number of all events, excepting cell aggregates and debris). FCM acquisitions were
495 performed on a FACS Canto II (BD Bioscience) using the DIVA software and further analyzed
496 with FlowJo (TreeStar).
497
498 **Multiplex immunoassay**
499 For multiplex assay, the fluidic fraction of BALs from mock controls and RSV-A2 were
500 collected. Cytokine concentrations were assessed using the MILLIPLEX® Ovine
501 Cytokine/Chemokine Panel 1 (Life Science Research) according to the manufacturer's
502 protocol and read on a Luminex MAGPIX® System including a xPONENT Software version
503 4.2 software (Luminex).
504
505 **Statistical Analysis**
506 Statistical analysis was done using the GraphPad Prism 8 software (GraphPad software, La
507 Jolla, CA, USA). Data are presented as box and whisker plots and to determine differences
508 between two groups, non-parametric paired Wilcoxon tests or Mann–Whitney U-tests were
509 used as appropriate. Associations were tested using the Spearman rank correlation test. A p
510 value < 0.05 was considered statistically significant.

511 **NOTES**

512 **Acknowledgements**

513 We thank Artur Summerfield, Christoph Aebi and Sean R. R. Hall for helpful discussions;
514 Sylvie Python, Aurélie Godel and Nathan Leborgne for technical assistance; Inês Berenguer
515 Veiga for participation in the animal trial; Hans Peter Lüthi, Roman Troxler, Jan Salchli, Daniel
516 Brechbühl and Katarzyna Sliz for animal care. The RSV isolate RSV-ON1-H1 was kindly
517 provided by Sibylle Haid, Martin Wetzke, Gesine Hansen and Thomas Pietschmann. T.D. was
518 supported in part by the EU FP7 Project UniVax (HEALTH-F3-2013-60173). This project was
519 funded by the Swiss National Science Foundation (grant No. 310030_172895 to M.P.A.).

520

521 **Data availability statement**

522 The data generated and analysed during the current study are available from the
523 corresponding author on reasonable request.

524

525 **Authors contribution**

526 All authors contributed to important elements to the work presented in this paper and reviewed
527 and approved the final version of this manuscript. T.D. designed the various antibody
528 combination staining, validated them *in vitro*, designed and performed the animal trials,
529 performed the RSV quantifications in animal tissues and serum micro-neutralization assays,
530 acquired, assembled, analyzed and interpreted the data, prepared the figures and wrote the
531 manuscript. M.B. and B.Z established the RSV quantification and serum micro-neutralization
532 assay protocols and designed and performed the animal trial. B.I.O.E. participated in the
533 execution of the animal trial. K.M. and H.P. participated in the execution of the animal trial and
534 evaluated the lung pathology. A.F. assisted in the animal trial and performed part of the
535 immunohistochemistry. L.B. computed the data from WBC and PMN counts in the circulation
536 with the R software and generated the related figures. A.T. helped with the multiplex assay.
537 C.B. helped with clinical observations, interpretation of the data, and reviewed the manuscript.

538 N.R. participated in the design and execution of the animal trial, organized the partitioning of
539 animals in stables, and monitored the clinical scores. M.P.A. conceived the idea, overviewed,
540 designed, led and performed the animal trial, and edited the manuscript.
541

542 **SUPPLEMENTARY MATERIAL**

543 Table S1. List of antibodies validated for their use in the study.
544 Table S2. Combination immunostainings used for the identification of cell subsets.
545 Figure S1. Longitudinal evaluation of peripheral blood over the course of RSV disease.
546 Figure S2. Evaluation of serum RSV-specific neutralizing antibodies.
547 Figure S3. RSV-specific neutralizing activity present in one uninfected animal.
548 Figure S4. FCM gating strategy for immune cells identification.
549 Figure S5. Neonatal RSV infection induces bronchoalveolar recruitment of activated pDCs.
550

551 **REFERENCES**

552 1. Shi T, McAllister DA, O'Brien KL, Simoes EAF, Madhi SA, Gessner BD, et al. Global,
553 regional, and national disease burden estimates of acute lower respiratory infections due to
554 respiratory syncytial virus in young children in 2015: a systematic review and modelling study.
555 Lancet. 2017;390(10098):946-58.

556 2. Pneumonia Etiology Research for Child Health Study G. Causes of severe pneumonia
557 requiring hospital admission in children without HIV infection from Africa and Asia: the PERCH
558 multi-country case-control study. Lancet. 2019;394(10200):757-79.

559 3. Nair H, Nokes DJ, Gessner BD, Dherani M, Madhi SA, Singleton RJ, et al. Global
560 burden of acute lower respiratory infections due to respiratory syncytial virus in young children:
561 a systematic review and meta-analysis. Lancet. 2010;375(9725):1545-55.

562 4. Hall CB, Weinberg GA, Iwane MK, Blumkin AK, Edwards KM, Staat MA, et al. The
563 burden of respiratory syncytial virus infection in young children. N Engl J Med.
564 2009;360(6):588-98.

565 5. Murray J, Bottle A, Sharland M, Modi N, Aylin P, Majeed A, et al. Risk factors for
566 hospital admission with RSV bronchiolitis in England: a population-based birth cohort study.
567 PLoS One. 2014;9(2):e89186.

568 6. Garcia CG, Bhore R, Soriano-Fallas A, Trost M, Chason R, Ramilo O, et al. Risk factors
569 in children hospitalized with RSV bronchiolitis versus non-RSV bronchiolitis. Pediatrics.
570 2010;126(6):e1453-60.

571 7. Hall CB, Weinberg GA, Blumkin AK, Edwards KM, Staat MA, Schultz AF, et al.
572 Respiratory syncytial virus-associated hospitalizations among children less than 24 months of
573 age. Pediatrics. 2013;132(2):e341-8.

574 8. Palivizumab, a Humanized Respiratory Syncytial Virus Monoclonal Antibody, Reduces
575 Hospitalization From Respiratory Syncytial Virus Infection in High-risk Infants. Pediatrics.
576 1998;102(3):531-7.

577 9. Openshaw PJM, Chiu C, Culley FJ, Johansson C. Protective and Harmful Immunity to
578 RSV Infection. Annu Rev Immunol. 2017;35:501-32.
579 10. Mold JE, Venkatasubrahmanyam S, Burt TD, Michaelsson J, Rivera JM, Galkina SA,
580 et al. Fetal and adult hematopoietic stem cells give rise to distinct T cell lineages in humans.
581 Science. 2010;330(6011):1695-9.
582 11. de Kleer IM, Kool M, de Bruijn MJ, Willart M, van Moorleghem J, Schuijs MJ, et al.
583 Perinatal Activation of the Interleukin-33 Pathway Promotes Type 2 Immunity in the
584 Developing Lung. Immunity. 2016;45(6):1285-98.
585 12. PrabhuDas M, Adkins B, Gans H, King C, Levy O, Ramilo O, et al. Challenges in infant
586 immunity: implications for responses to infection and vaccines. Nat Immunol. 2011;12(3):189-
587 94.
588 13. Dodd J, Riffault S, Kodituwakku JS, Hayday AC, Openshaw PJ. Pulmonary V gamma
589 4+ gamma delta T cells have proinflammatory and antiviral effects in viral lung disease. J
590 Immunol. 2009;182(2):1174-81.
591 14. Aoyagi M, Shimojo N, Sekine K, Nishimuta T, Kohno Y. Respiratory syncytial virus
592 infection suppresses IFN-gamma production of gammadelta T cells. Clin Exp Immunol.
593 2003;131(2):312-7.
594 15. Huang H, Saravia J, You D, Shaw AJ, Cormier SA. Impaired gamma delta T cell-
595 derived IL-17A and inflammasome activation during early respiratory syncytial virus infection
596 in infants. Immunol Cell Biol. 2015;93(2):126-35.
597 16. McGill JL, Sacco RE. gammadelta T cells and the immune response to respiratory
598 syncytial virus infection. Vet Immunol Immunopathol. 2016;181:24-9.
599 17. Restori KH, Srinivasa BT, Ward BJ, Fixman ED. Neonatal Immunity, Respiratory Virus
600 Infections, and the Development of Asthma. Front Immunol. 2018;9:1249.
601 18. Levy O. Innate immunity of the newborn: basic mechanisms and clinical correlates.
602 Nat Rev Immunol. 2007;7(5):379-90.

603 19. DeVincenzo JP, Wilkinson T, Vaishnaw A, Cehelsky J, Meyers R, Nochur S, et al. Viral
604 load drives disease in humans experimentally infected with respiratory syncytial virus. Am J
605 Respir Crit Care Med. 2010;182(10):1305-14.
606 20. Pino M, Kelvin DJ, Bermejo-Martin JF, Alonso A, Matias V, Tenorio A, et al.
607 Nasopharyngeal aspirate cytokine levels 1 yr after severe respiratory syncytial virus infection.
608 Pediatr Allergy Immunol. 2009;20(8):791-5.
609 21. Johnson JE, Gonzales RA, Olson SJ, Wright PF, Graham BS. The histopathology of
610 fatal untreated human respiratory syncytial virus infection. Mod Pathol. 2007;20(1):108-19.
611 22. Piedra PA. Clinical experience with respiratory syncytial virus vaccines. Pediatr Infect
612 Dis J. 2003;22(2 Suppl):S94-9.
613 23. Fishaut M, Tubergen D, McIntosh K. Cellular response to respiratory viruses with
614 particular reference to children with disorders of cell-mediated immunity. J Pediatr.
615 1980;96(2):179-86.
616 24. Roman M, Calhoun WJ, Hinton KL, Avendano LF, Simon V, Escobar AM, et al.
617 Respiratory syncytial virus infection in infants is associated with predominant Th-2-like
618 response. Am J Respir Crit Care Med. 1997;156(1):190-5.
619 25. Legg JP, Hussain IR, Warner JA, Johnston SL, Warner JO. Type 1 and type 2 cytokine
620 imbalance in acute respiratory syncytial virus bronchiolitis. Am J Respir Crit Care Med.
621 2003;168(6):633-9.
622 26. Siefker DT, Vu L, You D, McBride A, Taylor R, Jones TL, et al. Respiratory Syncytial
623 Virus Disease Severity Is Associated with Distinct CD8(+) T-Cell Profiles. Am J Respir Crit
624 Care Med. 2020;201(3):325-34.
625 27. Scheerlinck JP, Snibson KJ, Bowles VM, Sutton P. Biomedical applications of sheep
626 models: from asthma to vaccines. Trends Biotechnol. 2008;26(5):259-66.
627 28. Olivier A, Gallup J, de Macedo MM, Varga SM, Ackermann M. Human respiratory
628 syncytial virus A2 strain replicates and induces innate immune responses by respiratory
629 epithelia of neonatal lambs. Int J Exp Pathol. 2009;90(4):431-8.

630 29. Sitthicharoenchai P, Alnajjar S, Ackermann MR. A model of respiratory syncytial virus
631 (RSV) infection of infants in newborn lambs. Cell Tissue Res. 2020;380(2):313-24.
632 30. Derscheid RJ, Ackermann MR. Perinatal lamb model of respiratory syncytial virus
633 (RSV) infection. Viruses. 2012;4(10):2359-78.
634 31. Smit JJ, Rudd BD, Lukacs NW. Plasmacytoid dendritic cells inhibit pulmonary
635 immunopathology and promote clearance of respiratory syncytial virus. J Exp Med.
636 2006;203(5):1153-9.
637 32. McCarthy NE, Eberl M. Human gammadelta T-Cell Control of Mucosal Immunity and
638 Inflammation. Front Immunol. 2018;9:985.
639 33. Zhivaki D, Lemoine S, Lim A, Morva A, Vidalain PO, Schandene L, et al. Respiratory
640 Syncytial Virus Infects Regulatory B Cells in Human Neonates via Chemokine Receptor
641 CX3CR1 and Promotes Lung Disease Severity. Immunity. 2017;46(2):301-14.
642 34. Schmidt ME, Knudson CJ, Hartwig SM, Pewe LL, Meyerholz DK, Langlois RA, et al.
643 Memory CD8 T cells mediate severe immunopathology following respiratory syncytial virus
644 infection. PLoS Pathog. 2018;14(1):e1006810.
645 35. Liesman RM, Buchholz UJ, Luongo CL, Yang L, Proia AD, DeVincenzo JP, et al. RSV-
646 encoded NS2 promotes epithelial cell shedding and distal airway obstruction. J Clin Invest.
647 2014;124(5):2219-33.
648 36. Garcia-Mauriño C, Moore-Clingenpeel M, Thomas J, Mertz S, Cohen DM, Ramilo O,
649 et al. Viral Load Dynamics and Clinical Disease Severity in Infants With Respiratory Syncytial
650 Virus Infection. The Journal of infectious diseases. 2019;219(8):1207-15.
651 37. El Saleeby CM, Bush AJ, Harrison LM, Aitken JA, Devincenzo JP. Respiratory
652 syncytial virus load, viral dynamics, and disease severity in previously healthy naturally
653 infected children. The Journal of infectious diseases. 2011;204(7):996-1002.
654 38. Kerrin A, Fitch P, Errington C, Kerr D, Waxman L, Riding K, et al. Differential lower
655 airway dendritic cell patterns may reveal distinct endotypes of RSV bronchiolitis. Thorax.
656 2017;72(7):620-7.

657 39. Ruckwardt TJ, Malloy AM, Morabito KM, Graham BS. Quantitative and qualitative
658 deficits in neonatal lung-migratory dendritic cells impact the generation of the CD8+ T cell
659 response. PLoS Pathog. 2014;10(2):e1003934.
660 40. Johnson TR, Johnson CN, Corbett KS, Edwards GC, Graham BS. Primary human
661 mDC1, mDC2, and pDC dendritic cells are differentially infected and activated by respiratory
662 syncytial virus. PLoS One. 2011;6(1):e16458.
663 41. Kollmann TR, Crabtree J, Rein-Weston A, Blimkie D, Thommai F, Wang XY, et al.
664 Neonatal innate TLR-mediated responses are distinct from those of adults. J Immunol.
665 2009;183(11):7150-60.
666 42. Marr N, Wang TI, Kam SH, Hu YS, Sharma AA, Lam A, et al. Attenuation of respiratory
667 syncytial virus-induced and RIG-I-dependent type I IFN responses in human neonates and
668 very young children. J Immunol. 2014;192(3):948-57.
669 43. Danis B, George TC, Goriely S, Dutta B, Renneson J, Gatto L, et al. Interferon
670 regulatory factor 7-mediated responses are defective in cord blood plasmacytoid dendritic
671 cells. Eur J Immunol. 2008;38(2):507-17.
672 44. Lau-Kilby AW, Turfkruyer M, Kehl M, Yang L, Buchholz UJ, Hickey K, et al. Type I IFN
673 ineffectively activates neonatal dendritic cells limiting respiratory antiviral T-cell responses.
674 Mucosal Immunol. 2020;13(2):371-80.
675 45. De Weerd W, Twilhaar WN, Kimpen JL. T cell subset analysis in peripheral blood of
676 children with RSV bronchiolitis. Scand J Infect Dis. 1998;30(1):77-80.
677 46. Raiden S, Pandolfi J, Payaslian F, Anderson M, Rivarola N, Ferrero F, et al. Depletion
678 of circulating regulatory T cells during severe respiratory syncytial virus infection in young
679 children. Am J Respir Crit Care Med. 2014;189(7):865-8.
680 47. Thornburg NJ, Shepherd B, Crowe JE, Jr. Transforming growth factor beta is a major
681 regulator of human neonatal immune responses following respiratory syncytial virus infection.
682 J Virol. 2010;84(24):12895-902.

683 48. Durant LR, Makris S, Voorburg CM, Loebbermann J, Johansson C, Openshaw PJ.
684 Regulatory T cells prevent Th2 immune responses and pulmonary eosinophilia during
685 respiratory syncytial virus infection in mice. J Virol. 2013;87(20):10946-54.
686 49. Strickler HD, Martinson J, Desai S, Xie X, Burk RD, Anastos K, et al. The relation of
687 plasmacytoid dendritic cells (pDCs) and regulatory T-cells (Tregs) with HPV persistence in
688 HIV-infected and HIV-uninfected women. Viral Immunol. 2014;27(1):20-5.
689 50. Caballero MT, Serra ME, Acosta PL, Marzec J, Gibbons L, Salim M, et al. TLR4
690 genotype and environmental LPS mediate RSV bronchiolitis through Th2 polarization. J Clin
691 Invest. 2015;125(2):571-82.
692 51. Bermejo-Martin JF, Garcia-Arevalo MC, De Lejarazu RO, Ardura J, Eiros JM, Alonso
693 A, et al. Predominance of Th2 cytokines, CXC chemokines and innate immunity mediators at
694 the mucosal level during severe respiratory syncytial virus infection in children. Eur Cytokine
695 Netw. 2007;18(3):162-7.
696 52. Vu LD, Siefker D, Jones TL, You D, Taylor R, DeVincenzo J, et al. Elevated Levels of
697 Type 2 Respiratory Innate Lymphoid Cells in Human Infants with Severe Respiratory Syncytial
698 Virus Bronchiolitis. Am J Respir Crit Care Med. 2019;200(11):1414-23.
699 53. Hinks TSC, Hoyle RD, Gelfand EW. CD8(+) Tc2 cells: underappreciated contributors
700 to severe asthma. Eur Respir Rev. 2019;28(154).
701 54. Hebel K, Weinert S, Kuropka B, Knolle J, Kosak B, Jorch G, et al. CD4+ T cells from
702 human neonates and infants are poised spontaneously to run a nonclassical IL-4 program. J
703 Immunol. 2014;192(11):5160-70.
704 55. Bendelja K, Gagro A, Bace A, Lokar-Kolbas R, Krsulovic-Hresic V, Drazenovic V, et
705 al. Predominant type-2 response in infants with respiratory syncytial virus (RSV) infection
706 demonstrated by cytokine flow cytometry. Clin Exp Immunol. 2000;121(2):332-8.
707 56. Blockus S, Sake SM, Wetzke M, Grethe C, Graalmann T, Pils M, et al.
708 Labyrinthopeptins as virolytic inhibitors of respiratory syncytial virus cell entry. Antiviral Res.
709 2020;177:104774.

710 57. Gnanalingham MG, Mostyn A, Gardner DS, Stephenson T, Symonds ME.
711 Developmental regulation of the lung in preparation for life after birth: hormonal and nutritional
712 manipulation of local glucocorticoid action and uncoupling protein-2. J Endocrinol.
713 2006;188(3):375-86.
714 58. Mehinagic K, Pilo P, Vidondo B, Stokar-Regenscheit N. Coinfection of Swiss cattle with
715 bovine parainfluenza virus 3 and Mycoplasma bovis at acute and chronic stages of bovine
716 respiratory disease complex. J Vet Diagn Invest. 2019;31(5):674-80.
717 59. Lee DC, Harker JA, Tregoning JS, Atabani SF, Johansson C, Schwarze J, et al. CD25+
718 natural regulatory T cells are critical in limiting innate and adaptive immunity and resolving
719 disease following respiratory syncytial virus infection. J Virol. 2010;84(17):8790-8.
720 60. Vielle NJ, Zumkehr B, Garcia-Nicolas O, Blank F, Stojanov M, Musso D, et al. Silent
721 infection of human dendritic cells by African and Asian strains of Zika virus. Sci Rep.
722 2018;8(1):5440.
723 61. Sow FB, Gallup JM, Olivier A, Krishnan S, Patera AC, Suzich J, et al. Respiratory
724 syncytial virus is associated with an inflammatory response in lungs and architectural
725 remodeling of lung-draining lymph nodes of newborn lambs. Am J Physiol Lung Cell Mol
726 Physiol. 2011;300(1):L12-24.
727

728 **FIGURE LEGENDS**

729 **Figure 1. RSV infection is causing lower respiratory tract disease and leading to a**
730 **potentially protective humoral response.** (A) Illustration of the transtracheal RSV infection
731 experimental design. (B) RSV was quantified in the respiratory tract (BAL, cell fraction; Lung;
732 BAL, fluid) by qPCR. (C) RSV detection by immunohistochemistry in macrophages, and type
733 I pneumocytes. (D) Representative histological lung tissue sections from neonates over the
734 course of RSV infection (40X, HE). Lungs of RSV-infected animals (strain A2) show interstitial
735 septae expanded by inflammatory cells (interstitial pneumonia) and accumulation of
736 inflammatory cells within alveoli at days 3 and 6 p.i. No lesions at days 14 and 42 p.i. The
737 lungs of mock neonates allow comparison with normal lung architecture within the first weeks
738 of life. (E) Neonates infected with RSV can mount an antiviral neutralizing-antibody response.
739 (F) Anti-RSV Nabs persist over a 42-day long period. (G) Multiplex immunoassay using BAL
740 from the indicated animals. Heat map showing log_2-fold changes in concentration of 6
741 measured cytokines/chemokines normalized by mean value of control group: Mock, 3 days
742 p.i. Each symbol represents an individual animal (healthy adults, n=12; mock neonates, n=3
743 per time point; neonates infected with RSV, n=6 per time point). Boxplots indicate median
744 value (center line) and interquartile ranges (box edges), with whiskers extending to the lowest
745 and the highest values. Stars indicate significance levels. *, $p < 0.05$.

746

747 **Figure 2. Neonatal RSV infection activates a transient depletion of γδ T cells and**
748 **deficiency of IL-17-mediated immunity.** (A) Neonatal RSV infection induces a decrease in
749 γδ T cells number in the bronchoalveolar space, but not in the lung tissue. (B) Correlation
750 coefficient (r) obtained with in γδ T cell counts calculated as a function of % Live/Dead$^+$. (C-D)
751 Replenishment and maturation (CD25 up-regulation) of γδ T cell subset following the depletion
752 after RSV infection (C, representative FACS contour plots; D, Pie charts displaying all
753 individuals). (E) Inability of γδ T cells to produce IL-17 (representative FCM contour plots).
754 Each symbol represents an individual animal (healthy adults, n=12; mock neonates, n=3 per

755 time point; neonates infected with RSV, n=6 per time point). Boxplots indicate median value
756 (center line) and interquartile ranges (box edges), with whiskers extending to the lowest and
757 the highest values. Stars indicate significance levels. *, $p < 0.05$.
758
759 **Figure 3. Neonatal RSV infection induces a fast and massive Tc2 influx in the**
760 **bronchoalveolar space.** (A) RSV infection in neonate accelerates the recruitment of $CD4^+$ in
761 the bronchoalveolar space, but not in peribronchial LN or lung tissue. (B) RSV infection in
762 neonate induces a strong recruitment of $CD8^+$ T cells in the bronchoalveolar space, and to a
763 lesser extent in lung. (C-D) A high frequency of recruited $CD4^+$ T cells in bronchoalveolar
764 space differentiate towards a Th2 cytokine profile (IL-4 production) (C, representative FACS
765 contour plots; D, plot displaying all individuals). (E-F) A high frequency of recruited $CD8^+$ T
766 cells in bronchoalveolar space differentiate towards a Tc2 cytokine profile (IL-4 production) (E,
767 representative FCM contour plots; F, plot displaying all individuals). (G) RSV infection in
768 neonates modulates the activation (cell surface expression of CD25) and the maturation (cell
769 surface expression of T cell memory marker CD45RO) of $CD4^+$ and $CD8^+$ T cell pools in the
770 lung. Each symbol represents an individual animal (healthy adults, n=12; mock neonates, n=3
771 per time point; neonates infected with RSV, n=6 per time point). Boxplots indicate median
772 value (center line) and interquartile ranges (box edges), with whiskers extending to the lowest
773 and the highest values. Stars indicate significance levels. *, $p < 0.05$; **, $p < 0.01$; ***, $p <$
774 0.001.
775
776 **Figure 4. Neonatal RSV infection rapidly induces Treg suppressive functions to dampen**
777 **the Th2 and Tc2 responses.** (A) RSV infection in neonates led to the recruitment of Tregs in
778 the bronchoalveolar space, but not in peribronchial LN or lung tissue. (B) Progressive
779 decrease with age of Treg subset among the $CD4^+$ T cell fraction (representative FCM contour
780 plots). (C) Frequency of TGF-β-producing Tregs. (D) Correlation coefficient (r) obtained in
781 BALs with Treg counts calculated as a function of non-Treg $CD4^+$ counts (left), Treg counts
782 calculated as a function of $CD8^+$ counts (middle) and $CD8^+$ counts calculated as a function of

783 non-Treg $CD4^+$ counts (right). Significance was reached for the three correlations. Each
784 symbol represents an individual animal (healthy adults, n=12; mock neonates, n=3 per time
785 point; neonates infected with RSV, n=6 per time point). Boxplots indicate median value (center
786 line) and interquartile ranges (box edges), with whiskers extending to the lowest and the
787 highest values. Stars indicate significance levels. *, $p < 0.05$; **, $p < 0.01$.
788
789 **Figure 5. Distinct cellular immune response in neonates compare to adults following**
790 **RSV infection.** (A) RSV was quantified in the respiratory tract (BAL, cell fraction; lung; BAL,
791 fluid) of adults and neonates by qPCR. (B) Representative histological lung tissue sections
792 from RSV-infected neonates and adults at day 6 and 14 p.i. (40X, HE). Adults show no
793 histological lesions, whereas neonates show interstitial pneumonia at day 6.p.i. (C-D) Counts
794 of recruited pDCs and CD86 upregulation in bronchoalveolar space (C, plot displaying all
795 individuals; D, representative FCM contour plots). (E-G) $\gamma\delta$ T-cell counts, cytokine production,
796 and maturation in the bronchoalveolar space (E, plot displaying all individuals; F,
797 representative FCM contour plots; G, pie charts integrating all animals). (H-J) Recruitment,
798 activation, and maturation of the $CD4^+$ T-cell pool in the bronchoalveolar space (H, plot
799 displaying all individuals; I, representative FACS contour plots; J, pie charts integrating all
800 animals). (K-M) As in (H-J), but showing $CD8^+$ T-cell pool. (N-O) Recruitment of Tregs and
801 TGF-β production in the bronchoalveolar space (N, plot displaying all individuals; O,
802 representative FACS contour plots). Each symbol represents an individual animal (infected
803 adults, n=3 per time point; neonates infected with RSV, n=8 per time point). The grey zone
804 corresponds to the interval integrating the values of all corresponding mock controls. Boxplots
805 indicate median value (center line) and interquartile ranges (box edges), with whiskers
806 extending to the lowest and the highest values. Stars indicate significance levels. *, $p < 0.05$;
807 **, $p < 0.01$; ***, $p < 0.001$.
808
809 **Figure 6. The severity of disease relates to the magnitude of the unconventional**
810 **bronchoalveolar T cell responses.** (A) Representative histological lung tissue sections from

811 mock neonates and neonates infected with RSV-ON1-H1 and RSV A2 strain (40X, HE). At
812 day 6 p.i. the RSV-ON1-H1 infected animals show mild interstitial pneumonia (upper right
813 corner) with accumulation of inflammatory cells within alveoli. No lesions at day 14 p.i. or
814 mock-infected animals. (B) RSV was quantified in the respiratory tract (BAL, cell fraction) of
815 neonates infected with either RSV-ON1-H1 or RSV A2 strain by qPCR. (C) Comparison of
816 immune cell subset trafficking into bronchoalveolar space after infection with RSV-ON1-H1 or
817 RSV A2 strains. (D) Correlation coefficient (r) obtained in BALs with Treg counts calculated
818 as a function of pDC counts. Each symbol represents an individual animal (neonates infected
819 with RSV-ON1-H1, n=4 per time point; neonates infected with RSV-A2, n=8 per time point).
820 The grey zone corresponds to the interval integrating the values of all corresponding mock
821 controls. Boxplots indicate median value (center line) and interquartile ranges (box edges),
822 with whiskers extending to the lowest and the highest values. Stars indicate significance
823 levels. *, $p < 0.05$; **, $p < 0.01$; ***, $p < 0.001$.

A

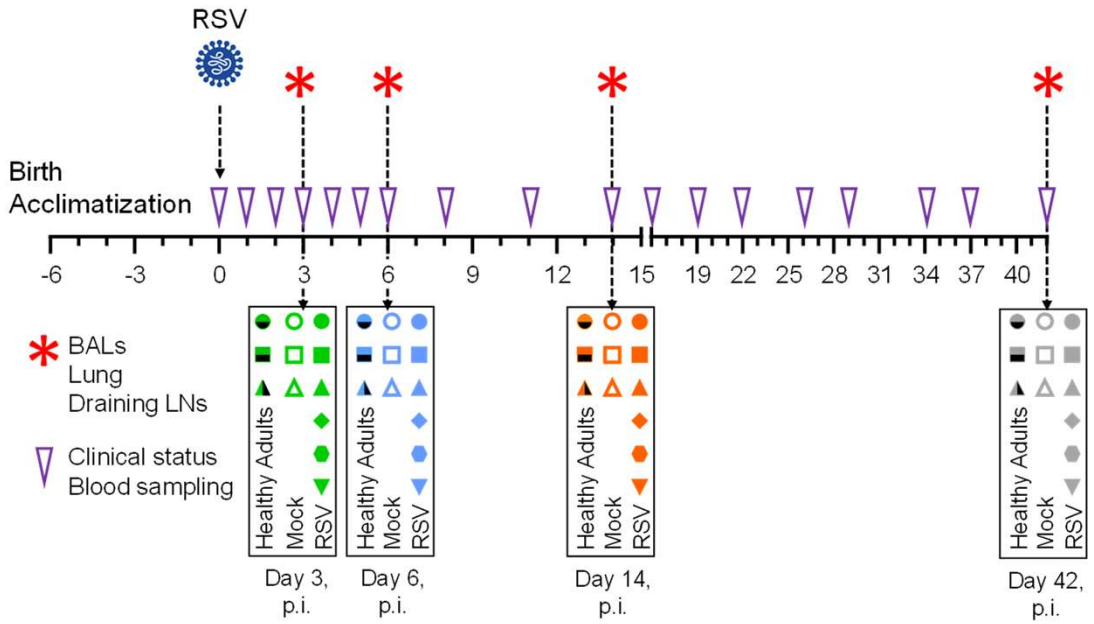
RSV
Birth
Acclimatization
-6
-3
0
3
6
9
12
15
19
22
25
28
31
34
37
40
BALs
Lung
Draining LNs
Clinical status
Blood sampling
Healthy Adults
Mock
RSV
Day 3, p.i.
Day 6, p.i.
Day 14, p.i.
Day 42, p.i.

B

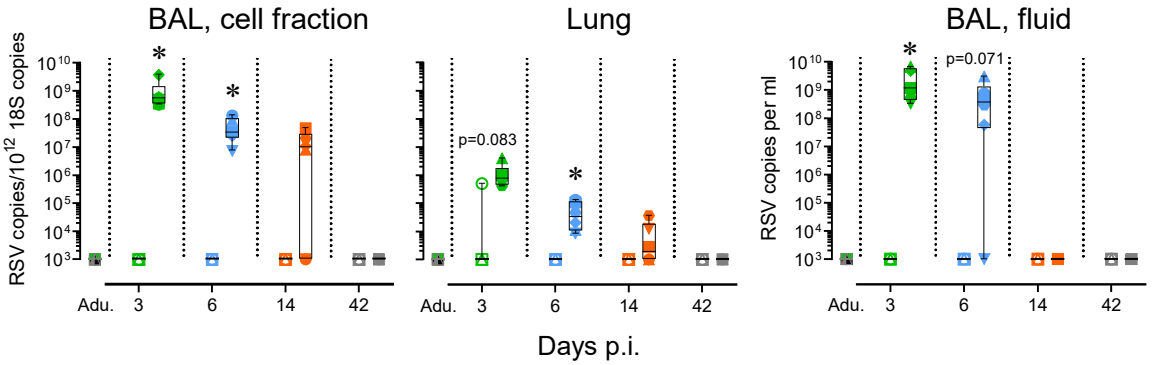
BAL, cell fraction
Lung
BAL, fluid
RSV copies/10^12 18S copies
RSV copies per ml
p=0.083
p=0.071
Adu.
3
6
14
42
Days p.i.

C

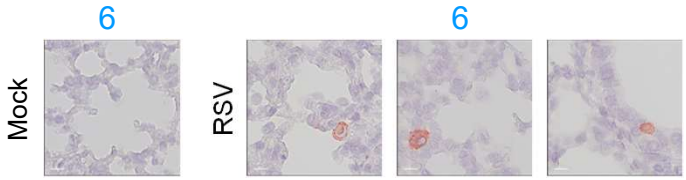
6
6
Mock
RSV

D

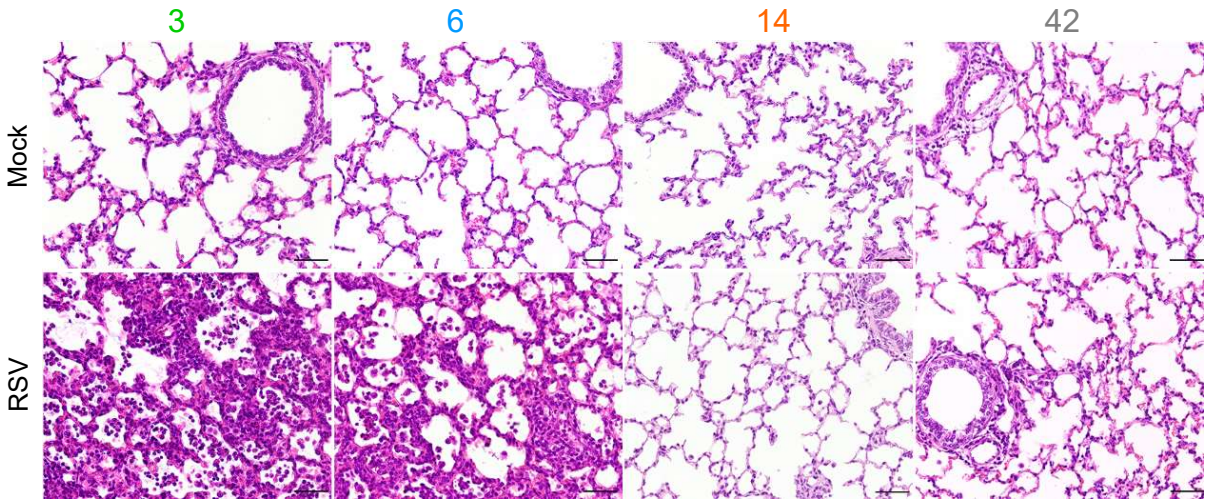
3
6
14
42
Mock
RSV

E

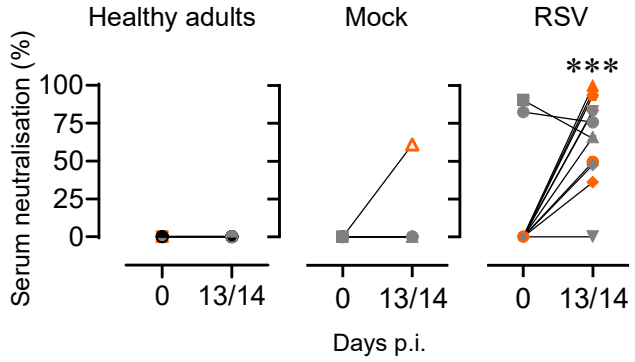
Healthy adults
Mock
RSV
Serum neutralisation (%)
100
75
50
25
0
***
0
13/14
Days p.i.

F

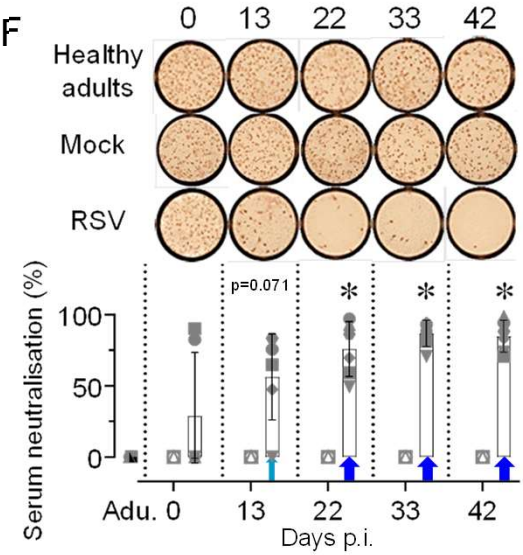
0
13
22
33
42
Healthy adults
Mock
RSV
Serum neutralisation (%)
100
50
0
p=0.071
*
Adu. 0
Days p.i.

G

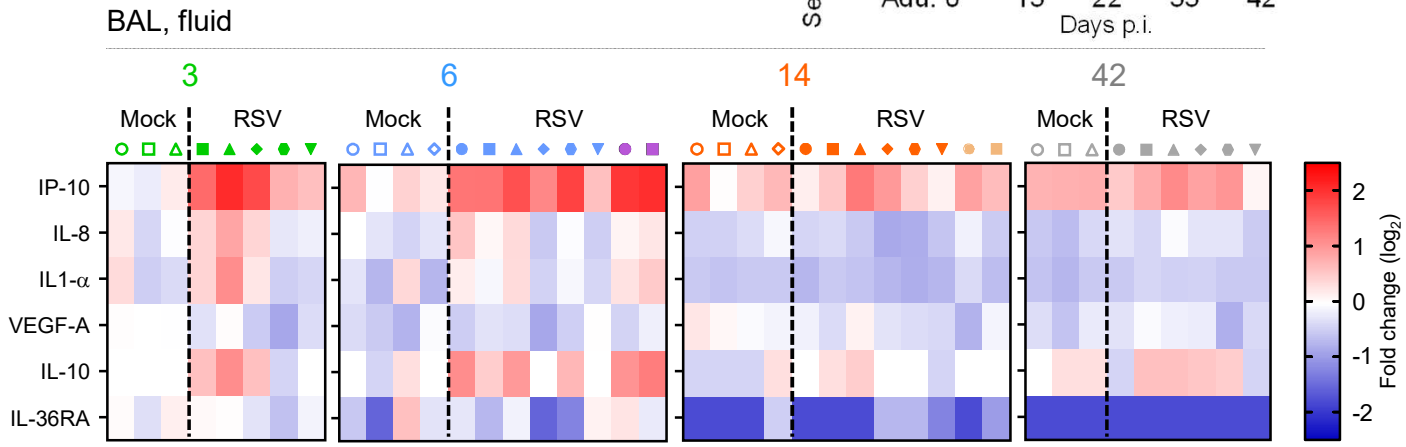
BAL, fluid
3
6
14
42
Mock
RSV
IP-10
IL-8
IL1-α
VEGF-A
IL-10
IL-36RA
2
1
0
-1
-2
Fold change (log2)

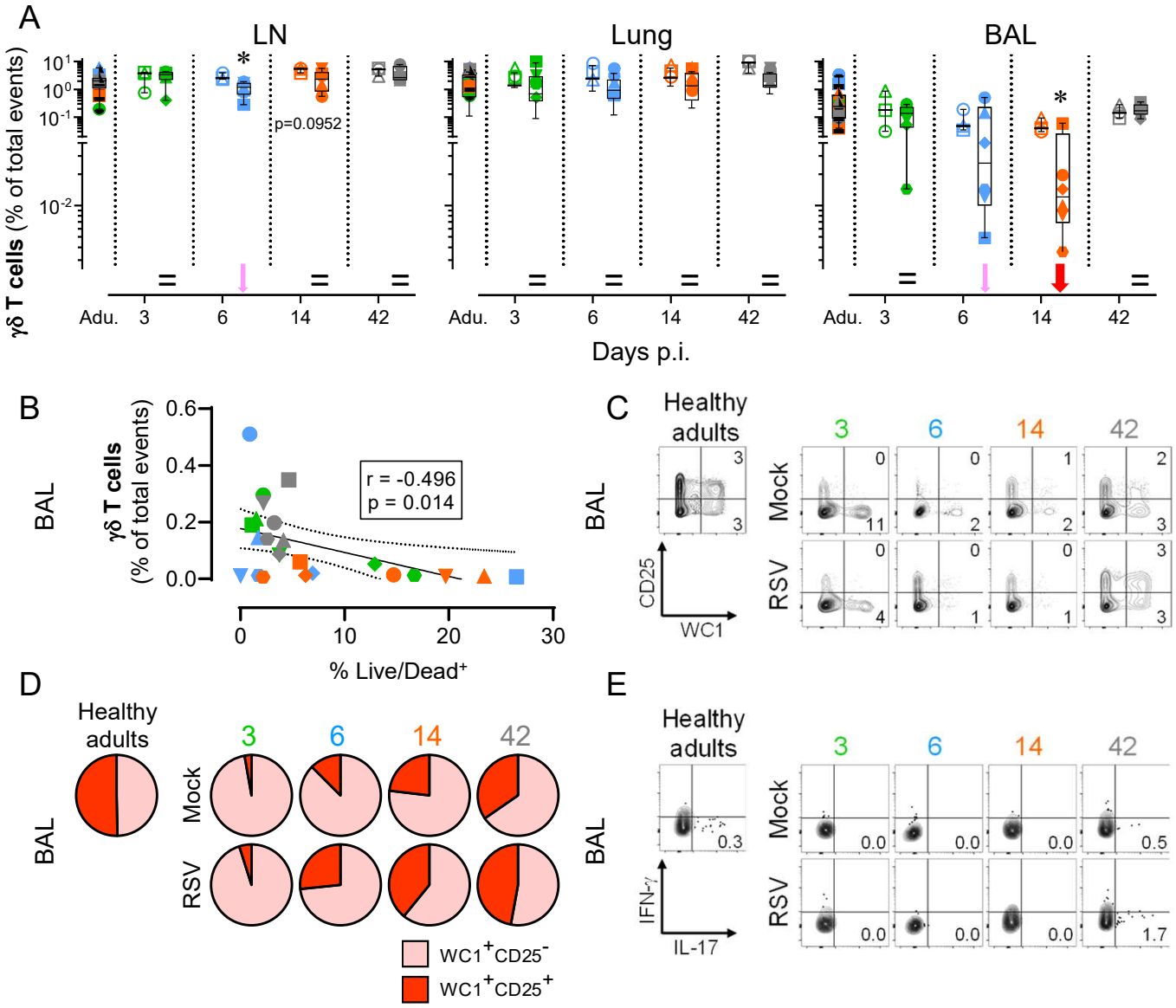
A
LN
Lung
BAL
γδ T cells (% of total events)
p=0.0952
Adu. 3 6 14 42
Days p.i.
B
BAL
γδ T cells (% of total events)
r = -0.496
p = 0.014
% Live/Dead+
C
Healthy adults
BAL
Mock
RSV
CD25
WC1
D
Healthy adults
BAL
Mock
RSV
WC1+CD25-
WC1+CD25+
E
Healthy adults
BAL
Mock
RSV
IFN-γ
IL-17

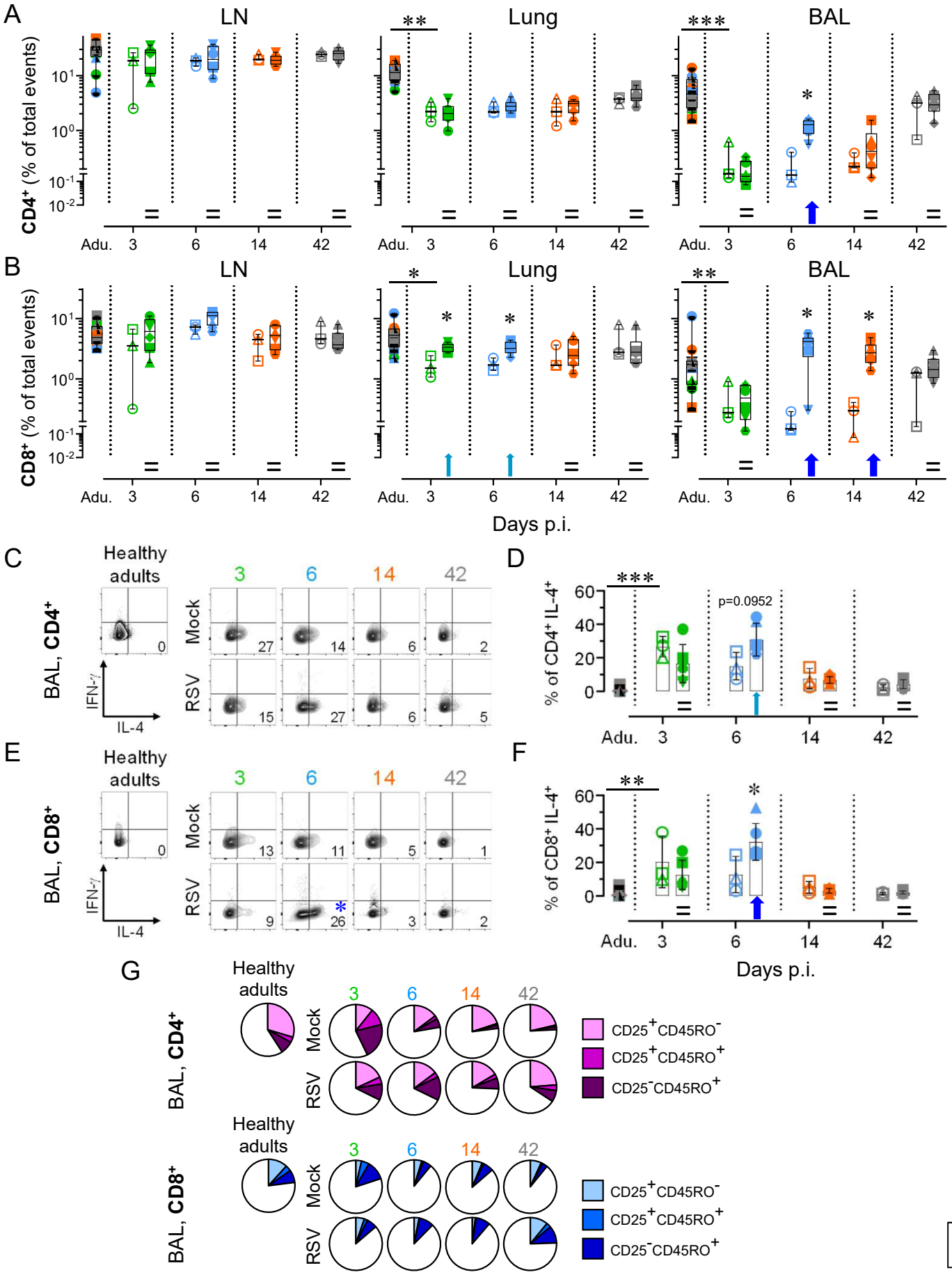
A
LN
Lung
BAL
CD4+ (% of total events)
Adu. 3 6 14 42
B
CD8+ (% of total events)
Days p.i.
C
Healthy adults
BAL, CD4+
Mock
RSV
IFN-γ
IL-4
D
% of CD4+ IL-4+
p=0.0952
E
BAL, CD8+
F
% of CD8+ IL-4+
G
BAL, CD4+
BAL, CD8+
CD25+CD45RO-
CD25+CD45RO+
CD25-CD45RO+

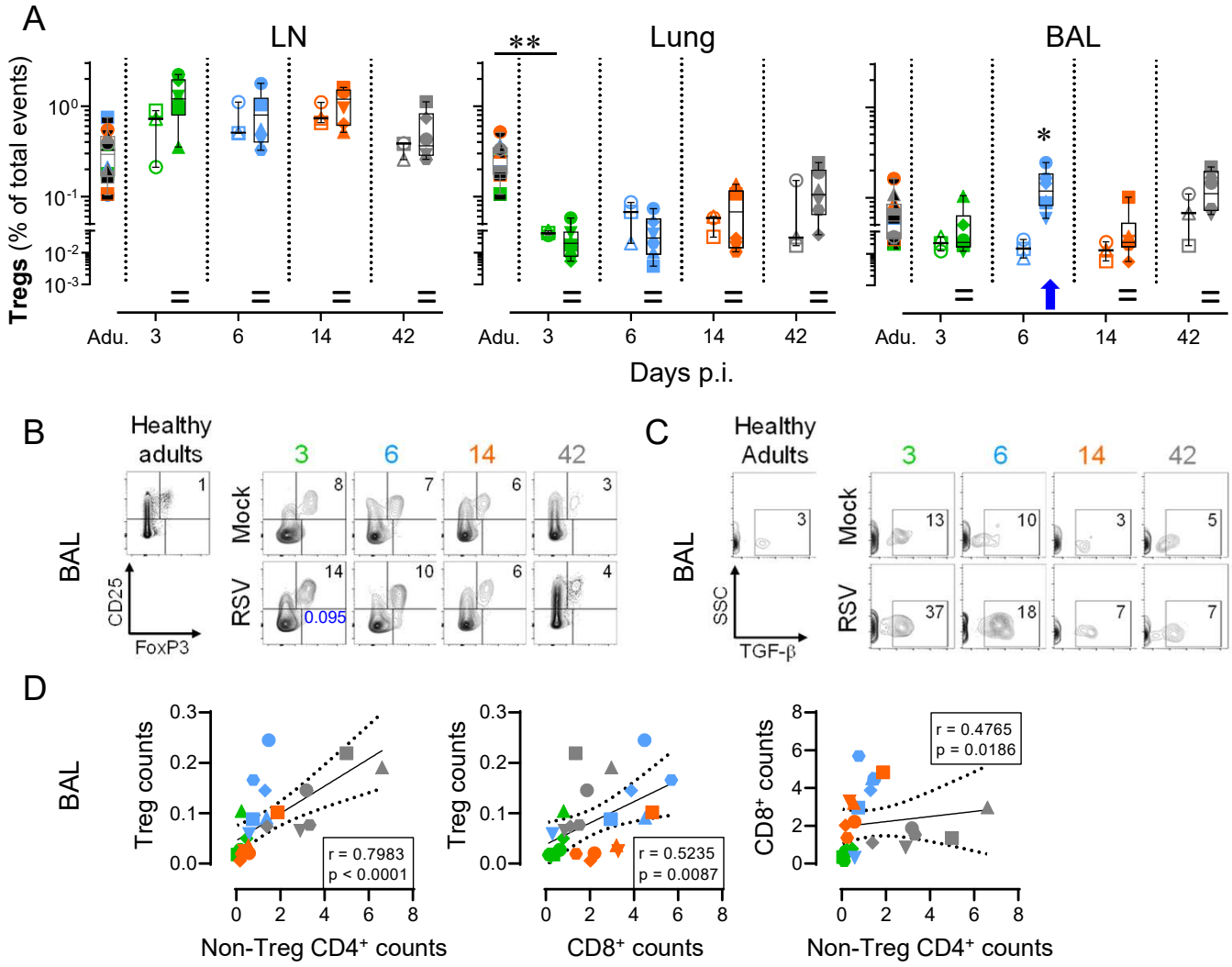
A
LN
Lung
BAL
Tregs (% of total events)
Adu.
3
6
14
42
Days p.i.
B
Healthy adults
BAL
Mock
RSV
CD25
FoxP3
0.095
C
Healthy Adults
SSC
TGF-β
D
Treg counts
Non-Treg CD4⁺ counts
CD8⁺ counts
r = 0.7983
p < 0.0001
r = 0.5235
p = 0.0087
r = 0.4765
p = 0.0186

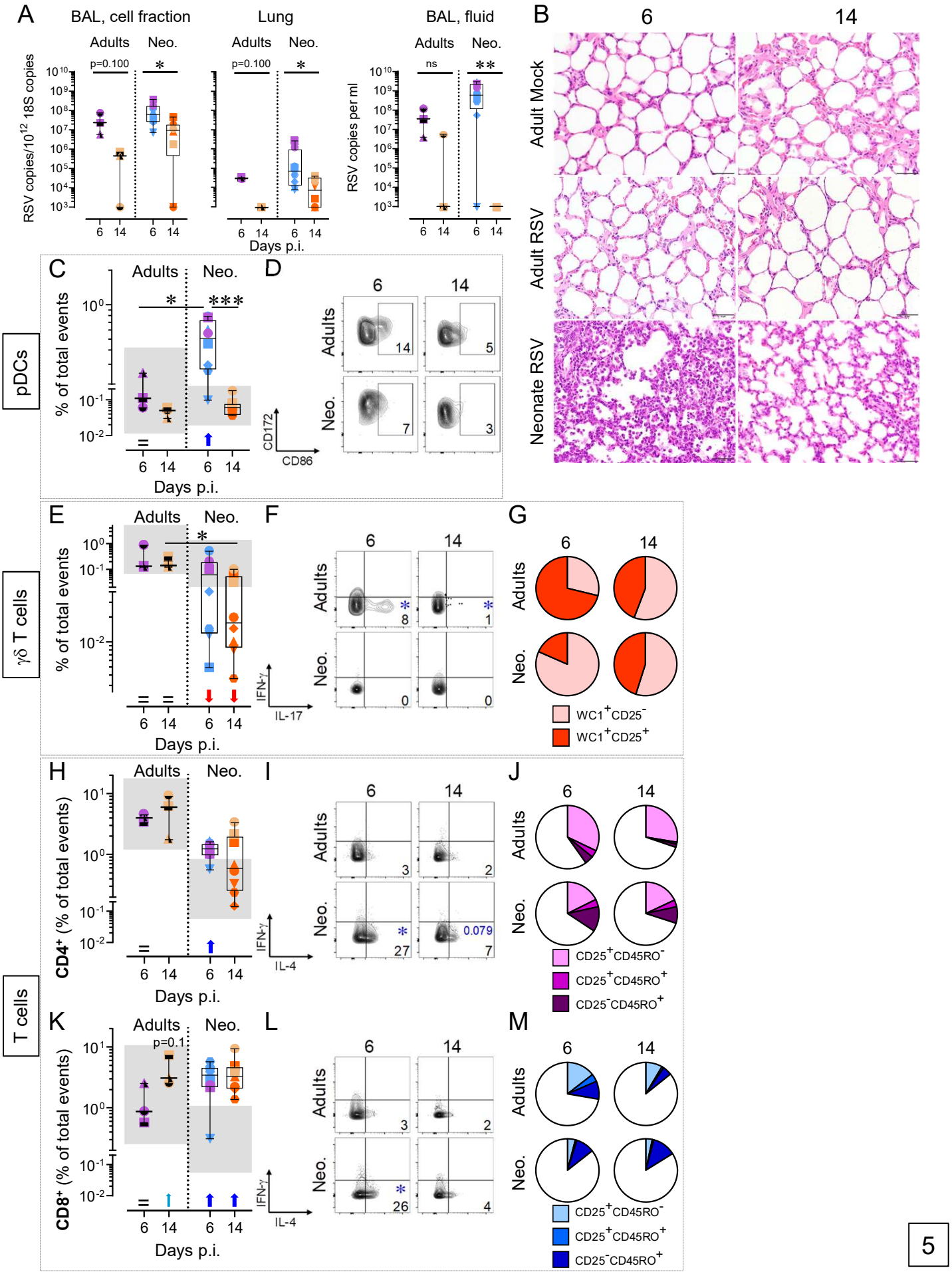
A
BAL, cell fraction
Lung
BAL, fluid
Adults
Neo.
p=0.100
*
ns
**
RSV copies/10^12 18S copies
RSV copies per ml
Days p.i.
B
6
14
Adult Mock
Adult RSV
Neonate RSV
pDCs
C
% of total events
***
D
CD172
CD86
γδ T cells
E
F
IFN-γ
IL-17
G
WC1+CD25-
WC1+CD25+
T cells
H
CD4+ (% of total events)
I
IL-4
J
CD25+CD45RO-
CD25+CD45RO+
CD25-CD45RO+
K
CD8+ (% of total events)
p=0.1
L
M

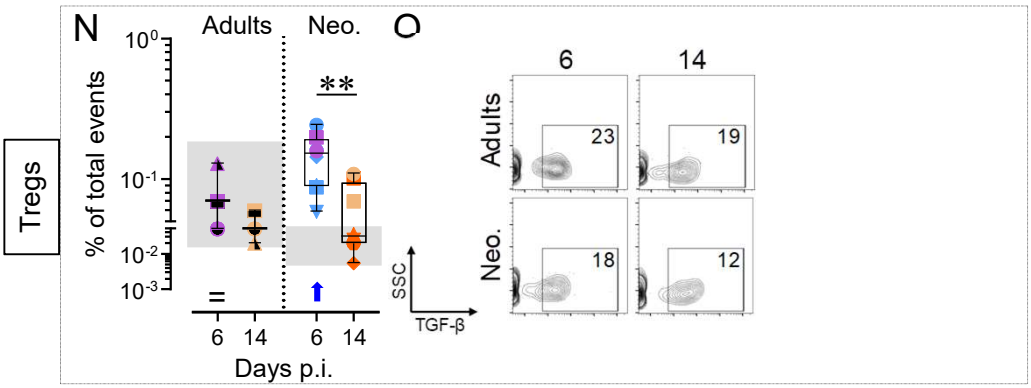
Tregs
N
Adults
Neo.
O
% of total events
10^0
10^{-1}
10^{-2}
10^{-3}
**
=
6
14
6
14
Days p.i.
SSC
TGF-β
6
14
Adults
Neo.
23
19
18
12

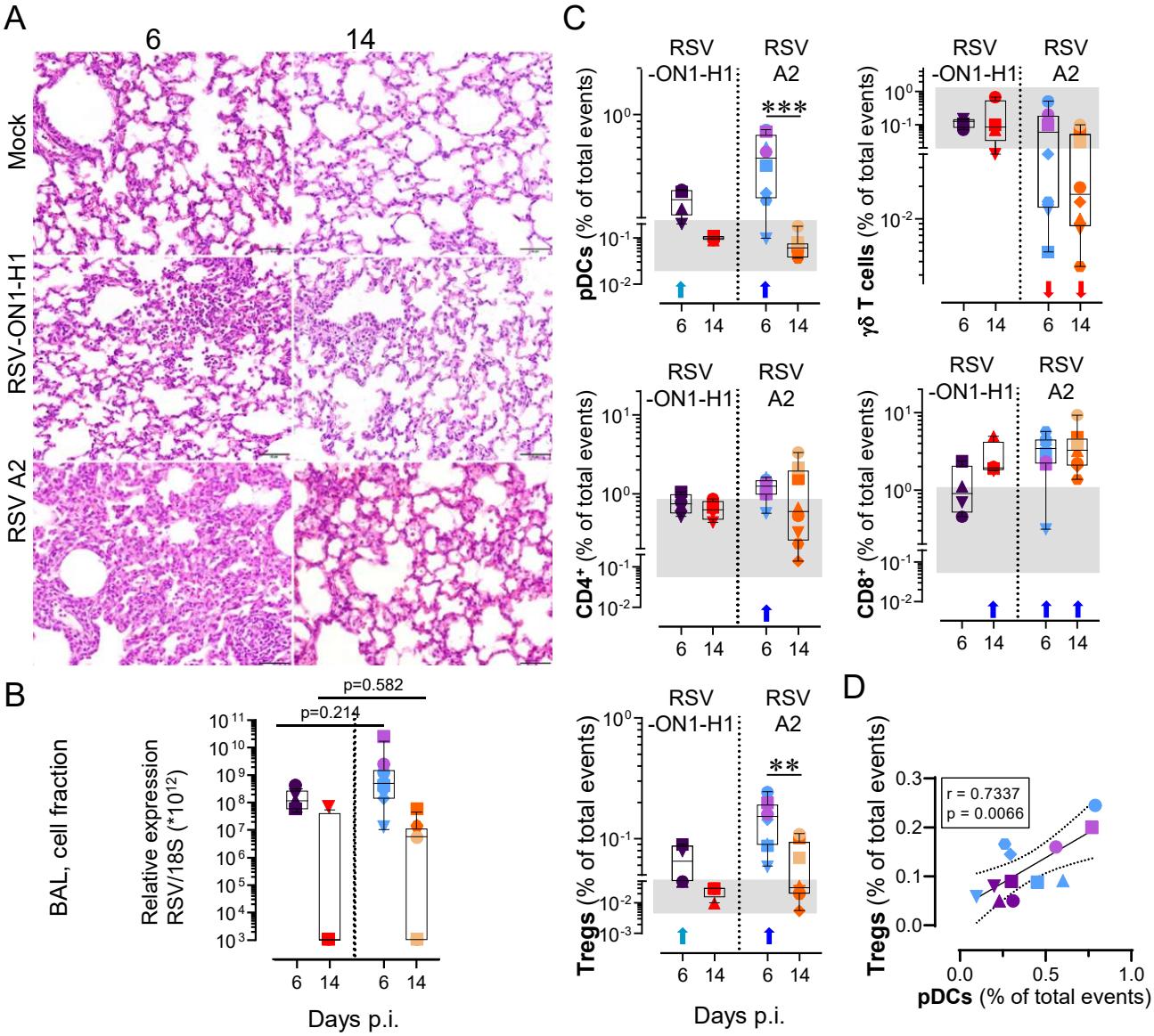
A
6
14
Mock
RSV-ON1-H1
RSV A2
B
BAL, cell fraction
Relative expression RSV/18S (*10^12)
p=0.582
p=0.214
Days p.i.
C
RSV -ON1-H1
RSV A2
pDCs (% of total events)
γδ T cells (% of total events)
CD4+ (% of total events)
CD8+ (% of total events)
Tregs (% of total events)
***
**
Days p.i.
D
r = 0.7337
p = 0.0066
Tregs (% of total events)
pDCs (% of total events)